

Fluid forces or impacts, what governs the entrainment of soil particles in sediment transport mediated by a Newtonian fluid?

Thomas Pähtz^{1,2*} and Orencio Durán³

1. *Institute of Port, Coastal and Offshore Engineering,
Ocean College, Zhejiang University, 310058 Hangzhou, China*

2. *State Key Laboratory of Satellite Ocean Environment Dynamics,
Second Institute of Oceanography, 310012 Hangzhou, China*

3. *Department of Physical Sciences, Virginia Institute of Marine Sciences,
College of William and Mary, 23062 Williamsburg, USA*

In steady sediment transport, the deposition of transported particles is balanced by the entrainment of soil bed particles by the action of fluid forces or particle-bed impacts. Here we propose a novel proxy to determine the role of impact entrainment relative to entrainment by the mean turbulent flow: the ‘bed velocity’ V_b , which is an effective near-bed-surface value of the average horizontal particle velocity that generalizes the classical slip velocity, used in studies of aeolian saltation transport, to sediment transport in an arbitrary Newtonian fluid. We study V_b for a wide range of the particle-fluid-density ratio s , Galileo number Ga , and Shields number Θ using direct sediment transport simulations with the numerical model of Durán et al. (Phys. Fluids **24**, 103306, 2012), which couples the Discrete Element Method for the particle motion with a continuum Reynolds-averaged description of hydrodynamics. We find that transport is fully sustained through impact entrainment (i.e., V_b is constant in natural units) when either the ‘impact number’ $Im = Ga\sqrt{s+0.5} \gtrsim 20$ or $\Theta \gtrsim 5/Im$. These conditions are obeyed for the vast majority of transport regimes, including steady turbulent bedload, which has long been thought to be sustained solely through fluid entrainment. In fact, we find transport is fully sustained through fluid entrainment (i.e., V_b scales with the near-bed horizontal fluid velocity) only for sufficiently viscous bedload transport at grain scale (i.e., for $Im \lesssim 20$ and $\Theta \lesssim 1/Im$). Finally, we do not find a strong correlation between, V_b , or the classical slip velocity, and the transport-layer-averaged horizontal particle velocity \bar{v}_x , which challenges the long-standing consensus that predominant impact entrainment is responsible for a linear scaling of the transport rate with Θ . For turbulent bedload in particular, \bar{v}_x increases with Θ despite V_b remaining constant, which we propose is linked to the formation of a liquid-like bed on top of the static-bed surface.

PACS numbers: 45.70.-n, 47.55.Kf, 92.40.Gc

I. INTRODUCTION

Sediment transport in a Newtonian fluid, such as water and air, is one of the most important geological processes responsible for the alteration of sea and riverscapes, and dry planetary surfaces [1–11]. It can occur in a large variety of natural environments: e.g., viscous and turbulent transport of minerals and organics by Earth’s water streams [1–5], and turbulent transport of dust and sand by Earth’s atmospheric winds [7–11].

Different sediment transport regimes are documented. Very small particles, whose weight can be fully supported by the fluid turbulence, tend to be transported in turbulent suspensions [5, 10]. Medium and large particles, on the other hand, are transported close to the surface, in trajectories not much influenced by fluid turbulence [5, 10]. The latter case includes bedload and saltation transport. Bedload transport refers to particles rolling, sliding, and hopping in the vicinity of the sediment bed, which is typical for the transport of sand and gravel by water streams [12, 13]. Saltation transport refers to particles moving in ballistic trajectories along the bed, which

is typical for the transport of sand by planetary winds [9–11].

It has become a widely-accepted hypothesis that the mechanisms sustaining bedload and saltation transport are fundamentally different: bedload transport being sustained through entrainment of soil bed particles directly by fluid forces [13–35] and saltation transport being sustained through particle-bed impacts ejecting bed particles [36–42], allowing transport even below the fluid entrainment threshold [9–11, 43–50]. However, recent studies have questioned this hypothesis by pointing out the role of particle inertia for sustaining bedload transport [51, 52].

Here we study the relevance of impact entrainment relative to direct entrainment by the mean turbulent flow in a unified manner using direct sediment transport simulations in a Newtonian fluid with the model of Ref. [53], which belongs to a new generation of sophisticated grain-scale models of sediment transport [9, 47, 50, 51, 53–70] and has been shown to reproduce many observations concerning viscous and turbulent sediment transport in air and water [9, 50, 53, 57] (e.g., see Fig. 6 of Ref. [57] and Figs. 6,7 of Ref. [50]), and bedform formation [58]. First, we present direct evidence from visual inspection of these simulations showing that impact entrainment events play

* 0012136@zju.edu.cn

a crucial role during both steady bedload and saltation transport. Then we quantitatively analyze the relative role of impact entrainment from our simulation data using a proxy that is similar, but not identical, to the classical slip velocity (i.e., the average horizontal particle velocity at the bed surface [9, 44–46, 48, 49, 71–75]). This analysis reveals a crucial influence of a novel dimensionless number, henceforth called ‘impact number’: $\text{Im} = \text{Ga}\sqrt{s+0.5}$, where $s = \rho_p/\rho_f$ is the particle-fluid density ratio and $\text{Ga} = \sqrt{(s-1)gd^3}/\nu$ the Galileo number (the square root of the Archimedes number), with g the gravitational constant, d the mean particle diameter, and ν the kinematic viscosity. Finally, we shed light on possible links between impact entrainment and average transport characteristics, such as the scaling of the sediment transport rate Q with the dimensionless fluid shear stress (the ‘‘Shields number’’ $\Theta = \tau/[(\rho_p - \rho_f)gd]$). In fact, it is a widespread believe that impact entrainment inevitably causes a (nearly) linear scaling $Q \propto \Theta - \Theta_t^*$, where Θ_t^* is the extrapolated value of Θ at which Q vanishes [38, 43–46, 48–50, 71, 76]. Here we challenge this believe.

The remainder of the manuscript is organized as follows. Section II briefly summarizes important details of the numerical model and explains how we calculate average quantities from the simulation data. Section III presents and discusses the evidence for impact entrainment in both bedload and saltation transport obtained from visualizations of the numerical simulations. Section IV represents the core of the paper. It introduces the proxy we use to quantify the relative role of impact entrainment, explains why other proxies, such as the slip velocity, are inappropriate, and analyzes our proxy over the entire range of simulated conditions. Section V discusses possible links between impact entrainment and average transport characteristics. Finally, we discuss our results and draw conclusions in Section VI.

II. NUMERICAL SIMULATIONS

The numerical model of sediment transport in Newtonian fluids of Ref. [53] couples a Discrete Element Method for the particle motion (≈ 15000 spheres, including > 10 layers of sediment bed particles) and a continuum Reynolds-averaged description of hydrodynamics. The Reynolds-Averaged Navier-Stokes equations are combined with an improved mixing length approximation, which can be used to calculate the mean turbulent fluid velocity at high particle concentrations. In contrast to the original model, which considers only gravity, buoyancy, and fluid drag forces acting on particles, we here also consider the added-mass force [9]. However, cohesive and higher-order fluid forces, such as the hindrance and lift force remain neglected. We also corrected two slight inaccuracies in the original model (with mostly negligible effect on the simulation outcome): We here take into account that the fluid shear stress is proportional to the

fluid volume fraction and neglect the buoyancy contribution from the divergence of the fluid shear stress because the divergence of the Reynolds stress, previously considered, actually does not contribute to the buoyancy force.

We would also like to emphasize that all results presented in this study for the bedload transport regime usually do not significantly depend on contact parameters, such as the restitution coefficient e and contact friction coefficient μ^c . For instance, bedload transport simulations with $e = 0.9$ and $e = 0.01$ are nearly exactly the same on average, which is consistent with previous reports [67]. This finding implies that any dissipative interaction force that is proportional to the relative velocity of two approaching particles and acts at and/or close to particle contact, such as the lubrication force [77], does not significantly influence average bedload transport characteristics as the effect of such forces can be incorporated in e and μ^c [62, 67, 78, 79].

We carry out simulations for s and Ga within the range $s \in [1.1, 10^7]$ and $\text{Ga} \in [0.1, 100]$. For each pair of s and Ga , we vary Θ in regular intervals above the entrainment cessation threshold Θ_t^e , which is usually larger than the rebound cessation threshold Θ_t^r associated with vanishing sediment transport [50]. We use the simulation data to compute local and transport layer averages of particle and fluid properties, such as the particle stress tensor, which is explained in the following.

A. Local, mass-weighted ensemble average

We compute the local, mass-weighted ensemble average $\langle A \rangle$ of a particle quantity A through [65]

$$\langle A \rangle = \frac{1}{\rho} \overline{\sum_n m^n A^n \delta(\mathbf{x} - \mathbf{x}^n)}^E, \quad (1)$$

$$\rho = \overline{\sum_n m^n \delta(\mathbf{x} - \mathbf{x}^n)}^E, \quad (2)$$

where ρ is the local particle mass density, m the particle mass, δ the delta distribution, and $\mathbf{x} = (x, y, z)$ (Cartesian coordinate system) the location, with x in flow direction parallel to the bed, z in direction normal to the bed oriented upwards, and y in lateral direction. Furthermore, the sum iterates over all particles ($n \in (1, N)$, with N the total number of particles), and $\overline{\cdot}^E$ denotes the ensemble average.

B. Particle stress tensor

Using the definition of the local mass-weighted ensemble average, we compute the particle stress tensor P_{ij}

from the simulation data through [65]

$$P_{ij} = \rho \langle v'_i v'_j \rangle + \frac{1}{2} \overline{\sum_{mn} F_j^{mn} (x_i^m - x_i^n) K(\mathbf{x}, \mathbf{x}^m, \mathbf{x}^n)}^E, \quad (3)$$

$$\mathbf{v}' = \mathbf{v} - \langle \mathbf{v} \rangle,$$

$$K = \int_0^1 \delta(\mathbf{x} - ((\mathbf{x}^m - \mathbf{x}^n)s' + \mathbf{x}^n)) ds',$$

where s' is a dummy variable, \mathbf{v} the particle velocity, and \mathbf{F}^{mn} the contact force applied by particle n on particle m ($\mathbf{F}^{mm} = 0$).

C. Transport layer average

We compute the transport layer average \bar{A} of a quantity A through

$$\bar{A} = \int_{z_r}^{\infty} \rho \langle A \rangle dz / \int_{z_r}^{\infty} \rho dz. \quad (4)$$

It describes a mass-weighted average of A over all particles within the transport layer ($z > z_r$), where the transport layer base height z_r is defined through

$$\max(P_{zz} \hat{\gamma}) = [P_{zz} \hat{\gamma}](z_r), \quad (5)$$

with $\hat{\gamma} = d\langle v_x \rangle / dz$ the particle shear rate. This definition is motivated by the fact that the term $P_{zz} \hat{\gamma}$ is the production rate of the cross-correlation fluctuation energy density $\rho \langle (v'_x v'_z) \rangle$ [65]. Because particle-bed rebounds are the main reason for the production of $\rho \langle (v'_x v'_z) \rangle$, since they effectively convert horizontal momentum of descending particles into vertical momentum of ascending particles, z_r is a measure for the effective location of energetic particle-bed rebounds.

III. VISUALIZATIONS OF IMPACT ENTRAINMENT EVENTS

Figure 1 shows snapshots of transport simulations near Θ_i^c for turbulent bedload transport (Fig. 1a) and saltation transport (Fig. 1b) shortly before and after an impact entrainment event (see also Movies S1 and S2). In both cases, a transported particle collides with one or more bed particles, which subsequently become mobilized with a short time delay. In bedload transport, the transported particle impacts the bed from a very small height and entrains a bed particle by dragging it out of its trap, while in saltation transport, the transported particle impacts the bed from a very large height and entrains a bed particle by ejecting it. Close to the threshold, impact entrainment events are rare in both cases as impacts occur much less often, but are much more effective, in saltation than they are in turbulent bedload transport

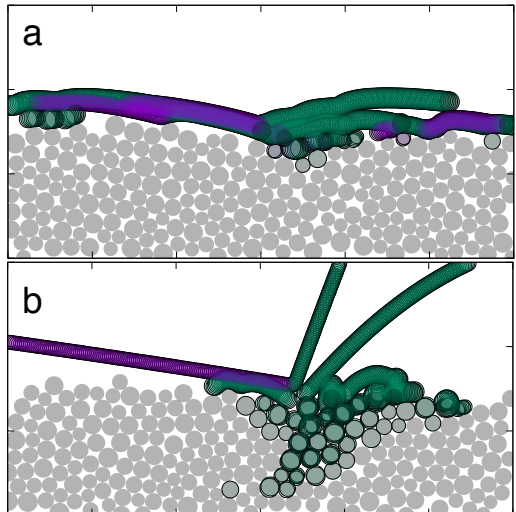


FIG. 1. Visualizations of impact entrainment events for (a) turbulent bedload and (b) saltation transport from direct sediment transport simulations near threshold conditions ($\Theta \cong \Theta_i^c$). The purple and green colors indicate the trajectory of particles before and after impact, respectively. Particles move from the left to the right.

(Movies S1 and S2). As a consequence, bed particles remain in repose most of the time as fluid forces are too weak to entrain them directly. Sufficiently far from the threshold, impact entrainment events occur much more often in saltation transport (Movie S3), whereas it is impossible to determine single entrainment events in turbulent bedload transport because several layers of the bed are in continuous motion (Movie S4). Note that movie captions are provided in Appendix A.

IV. PROXY FOR RELEVANCE OF IMPACT ENTRAINMENT RELATIVE TO FLUID ENTRAINMENT

The finding from the previous section that impact entrainment events play crucial roles during both saltation and turbulent bedload transport highlights the need for a proxy conveying information about the relevance of impact entrainment relative to direct entrainment by the mean turbulent flow. Here we discuss two potential proxies, which we obtain from the vertical profile of the average horizontal particle velocity $\langle v_x \rangle(z)$. Section IV A discusses the standard proxy, the slip velocity $\langle v_x \rangle(z_r)$, and why it is inappropriate for our purposes. Therefore, Section IV B proposes and quantitatively analyzes a novel proxy, the ‘bed velocity’.

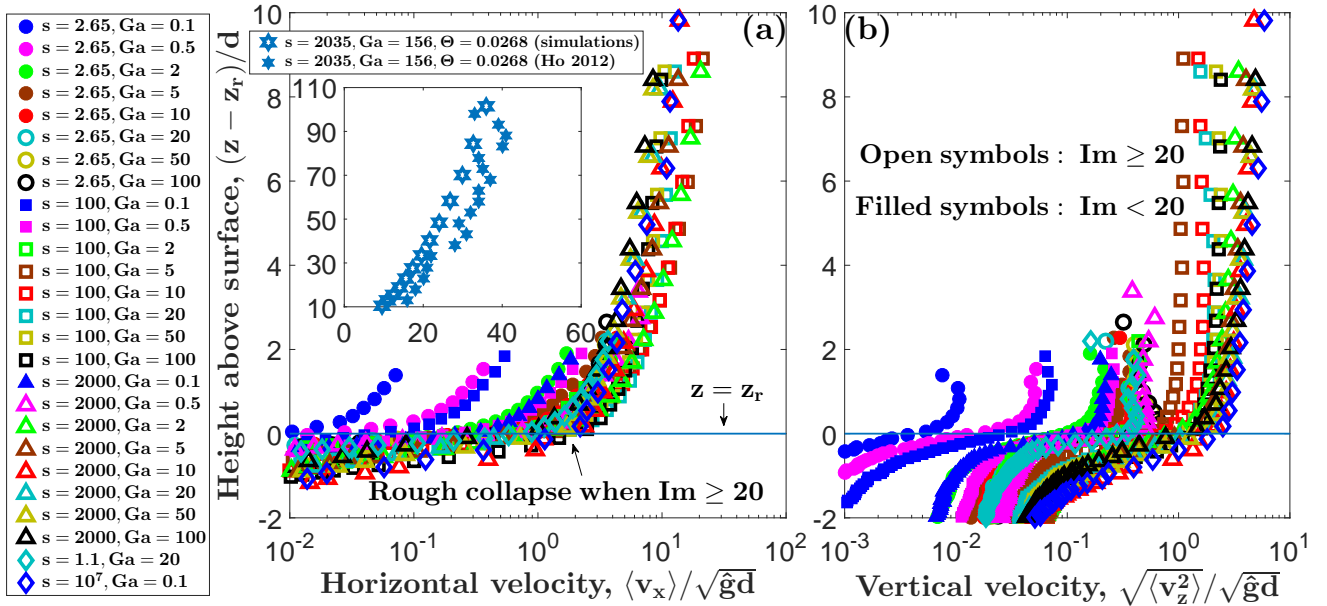


FIG. 2. Vertical profiles of (a) $\langle v_x \rangle / \sqrt{\hat{g}d}$ and (b) $\sqrt{\langle v_z^2 \rangle} / \sqrt{\hat{g}d}$ for various s and Ga near threshold conditions ($\Theta \approx \Theta_t^e$). Inset of (a): Comparison of simulated vertical profile of $\langle v_x \rangle(z_r) / \sqrt{\hat{g}d}$ with a profile measured in a wind tunnel by Ref. [80] for coarse sand ($d = 630 \mu\text{m}$).

A. Slip velocity

Figure 2 shows the vertical profiles of (a) $\langle v_x \rangle / \sqrt{\hat{g}d}$ and (b) $\sqrt{\langle v_z^2 \rangle} / \sqrt{\hat{g}d}$ relative to z_r for the entire simulated range of s and Ga , and a value of Θ that is near the associated entrainment threshold $\Theta_t^e(s, Ga)$, where $\hat{g} = (s+0.5)g/(s-1)$ is the value of g reduced by the buoyancy and added-mass force. It can be seen that there is a very rough tendency of $\langle v_x \rangle / \sqrt{\hat{g}d}$, but not of $\sqrt{\langle v_z^2 \rangle} / \sqrt{\hat{g}d}$, to collapse near z_r when the impact number $\text{Im} \gtrsim 20$ (open symbols). In the Aeolian Research community, a roughly constant value of $\langle v_x \rangle(z_r) / \sqrt{\hat{g}d}$ is thought to be evidence that saltation transport is a fully impact-sustained transport regime as it is associated with a constant average outcome of particle-bed impacts [9, 10, 44–46, 48, 49, 71–75]. In fact, when impact entrainment dominates fluid entrainment, every particle trapped at the bed must be replaced by precisely one particle entrained through impacts on average. However, this line of reasoning is not entirely accurate because it indirectly assumes that all particle-bed impacts occur at the same vertical location z_r . However, particle-bed impacts actually occur at varying vertical locations and their range of influence often involves several layers of the sediment bed (e.g., see Movie S3), which makes this assumption problematic because $\langle v_x \rangle(z)$ increases exponentially with z near z_r (Fig. 2a), meaning small changes of z have large effect. Indeed, Fig. 3a shows that the slip velocity exhibits significant fluctuations with ΘIm , and thus with Θ , even for typical saltation transport conditions in Earth’s atmosphere (e.g., $s = 2000$, $Ga \geq 10$). Note that

$\Theta \text{Im} = u_*^2 d / (\nu \sqrt{\hat{g}d})$, where $u_* = \sqrt{\tau / \rho_f}$, is the fluid shear velocity, is the viscous, horizontal near-bed fluid velocity in natural units ($\sqrt{\hat{g}d}$).

In the Aeolian Research community, it is the current consensus point of view that experiments (e.g., [80–87]) show an approximately constant slip velocity for saltation transport [10], which would contradict our numerical finding if true. However, what the experiments truly show is instead that the *extrapolation* of $\langle v_x \rangle(z)$ from vertical locations $z \gtrsim z_r + 5\text{mm}$ to z_r is approximately constant. In fact, reliable measurements of $\langle v_x \rangle(z) / \sqrt{\hat{g}d}$ do not exist for vertical locations $z \lesssim z_r + 5\text{mm}$ because large particle concentrations near z_r strongly disturb the measurement apparatuses [80], which is supported by the fact that the few actual measurements (i.e., non-extrapolations) of $\langle v_x \rangle(z) / \sqrt{\hat{g}d}$ reported for that region [81, 82, 85, 86] vary by more than an order of magnitude between about 0.5 [82] and 30 [85]. As shown in the inset of Fig. 2a, the data for $z \gtrsim z_r + 5\text{mm}$, where our simulations are consistent with measurements, suggest a linear trend of $\langle v_x \rangle(z)$ with z even though the actual trend for $z \lesssim z_r + 5\text{mm}$ is much closer to an exponential behavior. It explains why the extrapolation of $\langle v_x \rangle(z)$ to z_r yields values very different from the actual slip velocity. Indeed, when we estimate the slip velocity from our transport simulations via linear extrapolation, we obtain values that are consistent with the likewise extrapolated measurements (inset of Fig. 3a).

Though the extrapolation of $\langle v_x \rangle(z) / \sqrt{\hat{g}d}$ to z_r might serve as a proxy for the relative relevance of impact entrainment for saltation transport in Earth’s atmosphere, which is characterized by a large transport layer, it is

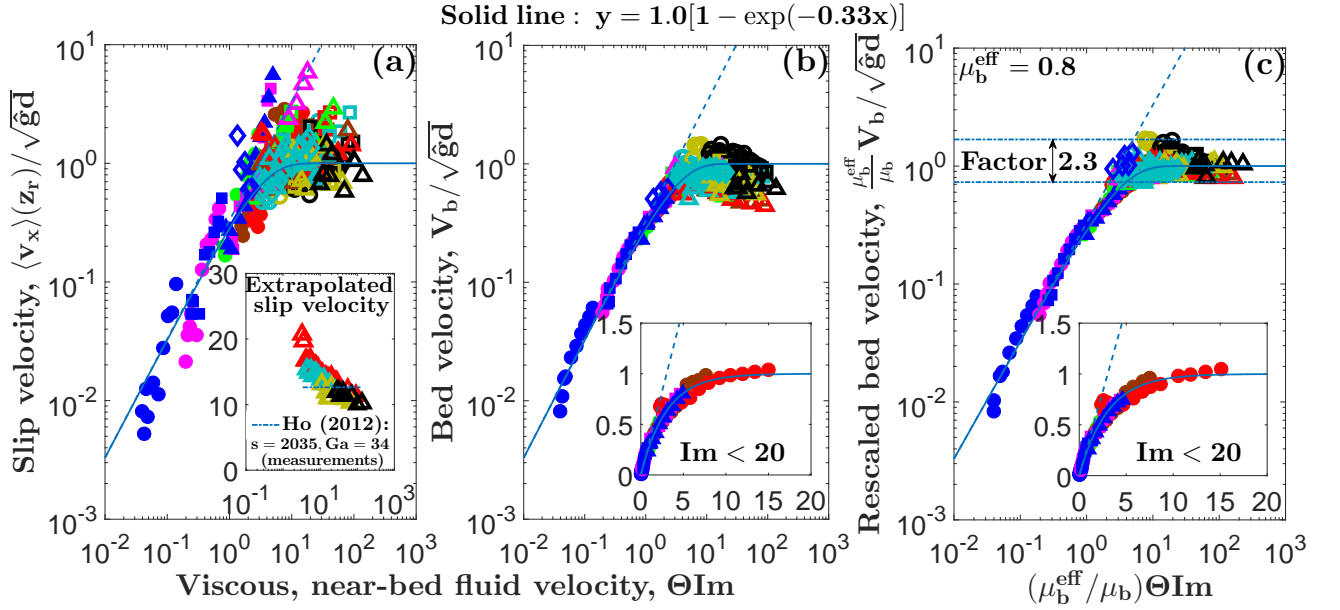


FIG. 3. (a) Dimensionless slip velocity $\langle v_x \rangle(z_r)/\sqrt{gd}$ and (b) dimensionless bed velocity V_b/\sqrt{gd} versus dimensionless, viscous, horizontal near-bed fluid velocity ΘIm for various s , Ga , and Θ in log-log scale. (c) Same as (b), but both axes are further rescaled by $\mu_b/0.8$. Inset of (a): Estimate of $\langle v_x \rangle(z_r)/\sqrt{gd}$ obtained from linear extrapolation of $\langle v_x \rangle(z)$ from $z \in (15, 110)d$ to z_r versus ΘIm for conditions with $s = 2000$, $\text{Ga} \geq 5$, and various Θ , and comparison to measurements by Ref. [80]. Insets of (b and c): Same as (b) and (c), but in linear-linear scale for cases with $\text{Im} < 20$. For symbol legend, see Fig. 2.

obviously meaningless for transport regimes with a small transport layer, such as bedload transport, and thus does not allow a unified treatment of all transport regimes. In what follows, we therefore propose a novel proxy.

B. Bed velocity

As explained above, the main issue with the slip velocity proxy is the fact that particle-bed impacts occur at varying vertical locations, rather than at a fixed vertical location z_r , and their range of influence often involves several layers of the sediment bed. To mend this issue, we here motivate the definition of an improved proxy, the bed velocity V_b , as an effective bed surface value of $\langle v_x \rangle$ that involves several layers around z_r .

First, we use that $\langle v_x \rangle$ exponentially decays within the sediment bed with a characteristic decay height proportional to d (Fig. 2a). An effective value of $\langle v_x \rangle$ must thus be proportional to an effective value V'_b of the horizontal velocity gradient $\dot{\gamma}$ near the bed surface:

$$V_b \propto V'_b d. \quad (6)$$

Second, we calculate V'_b as the ratio between $[-P_{zx}\dot{\gamma}](z_r)$, which is a suitable definition of an effective bed surface value of $-P_{zx}\dot{\gamma}$ (cf. Eq. (5)), and a suitable definition of the bed-surface-averaged particle shear stress $-P_{zx}$,

namely,

$$V'_b = \frac{[-P_{zx}\dot{\gamma}](z_r)}{\frac{1}{\rho_b} \int_{-\infty}^{\infty} \frac{d\rho}{dz} P_{zx} dz}, \quad (7)$$

where the weight $-\rho_b^{-1} d\rho/dz$, with $\rho_b \approx 0.58\rho_p$ the value of the particle concentration ρ deep within the bed, is maximal near the bed surface as it vanishes sufficiently within and above the bed. After partial integration, using $-P_{zx}(-\infty) = \tau$ and the horizontal momentum balance $dP_{zx}/dz = \rho\langle a_x \rangle$ [65], with \mathbf{a} the particle acceleration due to the action of non-contact forces, Eq. (7) becomes

$$V'_b = \frac{[-P_{zx}\dot{\gamma}](z_r)}{\tau - \frac{1}{\rho_b} \int_{-\infty}^{\infty} \rho^2 \langle a_x \rangle dz}. \quad (8)$$

Finally, we obtain the proportionality factor in Eq. (6) by imposing that the bed velocity very roughly equals the classical slip velocity, $V_b \approx \langle v_x \rangle(z_r)$, for the simulated turbulent saltation transport cases ($s = 2000$, $\text{Ga} \geq 10$). This constraint yields

$$V_b = 0.33d \times \frac{[-P_{zx}\dot{\gamma}](z_r)}{\tau - \frac{1}{\rho_b} \int_{-\infty}^{\infty} \rho^2 \langle a_x \rangle dz}. \quad (9)$$

Figure 3b shows that V_b/\sqrt{gd} is a much better proxy than $\langle v_x \rangle(z_r)/\sqrt{gd}$ (Fig. 3a) as it reproduces the approximately constant behavior expected for saltation transport in Earth's atmosphere. In detail, we observe two

extreme regimes. When sediment transport is fully sustained through direct entrainment by the mean turbulent flow, the bed velocity scales with the average near-bed fluid velocity (dashed line in Fig. 3b). In contrast, when sediment transport is fully sustained through impact entrainment, the dimensionless bed velocity does not change much with Θ , s , and Ga : $V_b/\sqrt{\hat{g}d} \approx 1.0$. A part of the variation of $V_b/\sqrt{\hat{g}d}$ in this regime can be attributed to small changes of the bed friction coefficient $\mu_b = \mu(z_r)$, where $\mu = -P_{zx}/P_{zz}$. In fact, we find that assuming $V_b/\sqrt{\hat{g}d} \propto \mu_b$ for fully impact-sustained conditions results in a significantly improved data collapse (Fig. 3c), which makes sense because one can expect that impact entrainment is the more difficult (larger $V_b/\sqrt{\hat{g}d}$) the larger the granular resistance at the bed surface (larger μ_b). Note that Fig. 3c corresponds to Fig. 3b when setting $\mu_b = 0.8 = \text{const}$.

The transition to a fully impact-sustained transport regime is determined by two independent conditions. First, the impact number has to exceed a critical value: $\text{Im} \gtrsim 20$ (Fig. 3, open symbols). This follows from the fact that the transport-layer average \bar{v}_x of the horizontal particle velocity must be larger than the bed velocity as $\langle v_x \rangle(z)$ increases with z . For relatively viscous conditions at grain scale ($Ga < 5$) and close to the entrainment threshold (Θ_t^e), the scaling of the average particle velocity \bar{v}_x can be obtained from the proportionality of \bar{v}_x with the transport-layer-averaged fluid velocity \bar{u}_x (Fig. 6) and a dynamic-friction condition (i.e., $\bar{u}_x - \bar{v}_x \propto Ga\sqrt{(s-1)gd}$ [50]). Thus, $\bar{v}_x \propto Ga\sqrt{(s-1)gd} = \text{Im}\sqrt{\hat{g}d}$ and the condition $\bar{v}_x > V_b \approx \sqrt{\hat{g}d}$ implies $\text{Im} > \text{Im}_c$, with $\text{Im}_c \approx 20$.

The second condition for fully impact-sustained transport is $\Theta \gtrsim 5/\text{Im}$ and follows from the proportionality of the dimensionless bed velocity with the dimensionless near-bed fluid velocity in the fully fluid-sustained regime ($V_b/\sqrt{\hat{g}d} \propto \Theta \text{Im}$) and the fact that $V_b/\sqrt{\hat{g}d}$ cannot increase indefinitely (Figs. 3b,c). Therefore, for $\text{Im} < 20$, which exclusively characterizes viscous bedload transport conditions, increasing the Shields parameter leads to a transition from fully fluid-sustained transport when $\Theta \lesssim 1/\text{Im}$ to fully impact-sustained transport when $\Theta \gtrsim 5/\text{Im}$ as the increasing bed velocity reaches the maximum value needed to replace every particle trapped at the bed by exactly one particle entrained through impacts (insets of Figs. 3b,c). Note that, near the threshold, the condition $\Theta \gtrsim 5/\text{Im}$ always implies $\text{Im} \gtrsim 20$ (i.e., $\Theta_t^e < 0.2$ [88]), but not vice versa (e.g., $s = 10^7$, $Ga = 0.1$ in Figs. 3b,c), and the condition $\text{Im} \lesssim 4$ always implies $\Theta \lesssim 1/\text{Im}$.

V. LINK BETWEEN BED VELOCITY AND AVERAGE TRANSPORT CHARACTERISTICS

It is commonly argued that the average horizontal particle velocity \bar{v}_x in the fully impact-sustained regime is constant [38, 46, 48, 49] or nearly constant [43–45, 71, 76],

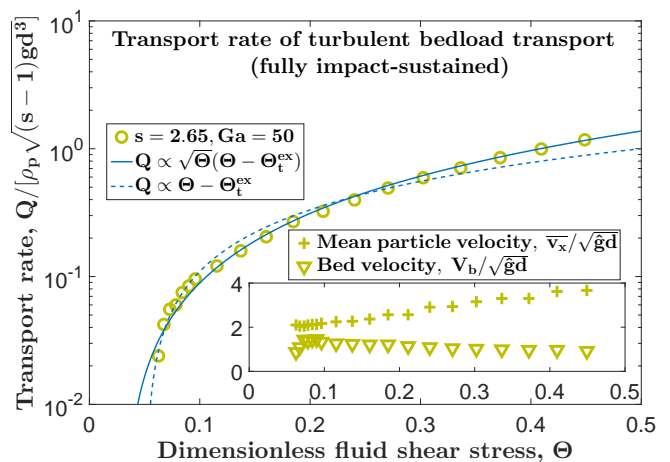


FIG. 4. Dimensionless sediment transport rate $Q/[\rho_p\sqrt{(s-1)gd^3}]$ versus dimensionless fluid shear stress Θ for fully impact-sustained bedload transport ($s = 2.65$ and $Ga = 50$). Inset: Dimensionless transport-layer-averaged horizontal particle velocity $\bar{v}_x/\sqrt{\hat{g}d}$ and bed velocity $V_b/\sqrt{\hat{g}d}$ versus Θ .

and that the sediment transport rate therefore approximately scales as $Q \propto \Theta - \Theta_t^r$, because the slip velocity is constant. In light of our finding of a generally non-constant slip velocity, but constant bed velocity V_b , in the fully impact-sustained regime (Fig. 3), one should actually rephrase this argument and say that \bar{v}_x is constant because the bed velocity V_b is constant in this regime. However, even when rephrased, we find that this argument is not valid for fully impact-sustained bedload transport (Fig. 4). Although Q is, indeed, linear in Θ when $\Theta \lesssim 2\Theta_t^r$, it transforms into a $\Theta^{1.5}$ -dependency when $\Theta \gtrsim 2\Theta_t^r$. As a consequence, the scaling $Q \propto \sqrt{\Theta}(\Theta - \Theta_t^r)$, which is consistent with measurements of the bedload transport rate [89–91], provides a much better overall fit to the simulations.

The transition from a linear to a non-linear transport law for turbulent bedload transport is consistent with a transition from a constant average particle velocity \bar{v}_x to one that increases with Θ , which occurs even though V_b remains nearly constant (inset of Fig. 4). A similar transition in $\bar{v}_x(\Theta)$ can be found for some other fully impact-sustained conditions (Fig. 7b) and a similar lack of correlation of \bar{v}_x with V_b for all fully impact-sustained conditions (Fig. 5a). Also the classical slip velocity $\langle v_x \rangle(z_r)$ usually does not correlate with \bar{v}_x (Fig. 5b) with the exception of bedload transport conditions (Fig. 5c).

Rather than with the bed velocity, the horizontal particle velocity scales with the horizontal fluid velocity (Fig. 6). In detail, we find that the scaling of \bar{v}_x depends on the relation between \bar{v}_x and the size of the transport layer $(\bar{z} - z_r)$. When the transport layer is within the viscous sublayer of the turbulent boundary layer ($(\bar{z} - z_r)/z_\nu \lesssim 5$, with the viscous length $z_\nu \equiv d/[\sqrt{\Theta}Ga]$), \bar{v}_x scales with the characteristic fluid

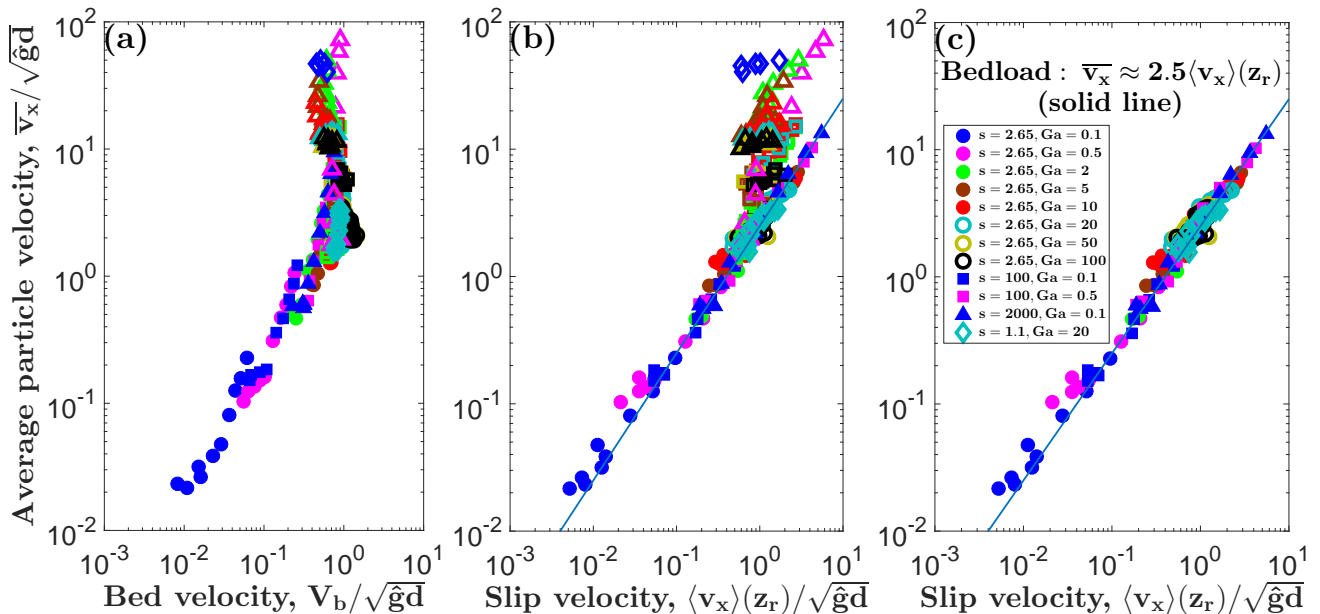


FIG. 5. Correlation between average horizontal particle velocity \bar{v}_x and (a) bed velocity V_b and (b) slip velocity $\langle v_x \rangle(z_r)$. (c) Same as (b), but only for bedload transport conditions. For symbol legend, see Fig. 2.

velocity within the viscous sublayer: $\bar{v}_x \propto \bar{u}_x$, where \bar{u}_x scales as $\bar{u}_x \approx \sqrt{\Theta(s-1)gd(\bar{z} - z_r)}/z_\nu$ when the particle-flow feedback (see below) can be neglected. On the other hand, when the transport layer extends beyond the viscous sublayer, the scale of the particle velocity is dominated by the characteristic fluid velocity in the logarithmic region of the velocity profile. That is, $\bar{v}_x \propto \sqrt{\Theta(s-1)gd} \equiv u_*$ when the particle-flow feedback can be neglected.

However, for saltation transport in Earth's atmosphere ($s = 2000$, $Ga \gtrsim 10$), it is well-known that there is a strong negative feedback on the flow generated by particle motion [92–94], which is a necessary condition to maintain a constant average impact velocity [9, 10]. As a consequence, the fluid shear velocity remains approximately constant with Θ in an extended region above the bed surface, and the particle velocity scales as $\bar{v}_x \propto \sqrt{\Theta_t^r(s-1)gd} \equiv u_t^r$ (inset of Fig. 6), resulting in a linear scaling of Q with Θ , consistent with measurements [86, 87, 95, 96]. We propose that the same negative feedback keeps a constant average particle velocity, at least close enough to the threshold, in all fully impact-sustained regimes (inset of Fig. 6), including turbulent bedload transport. However, the simulations suggest that, at sufficiently large fluid shear stresses ($\Theta \gtrsim 2\Theta_t^r$ for turbulent bedload transport), a highly collisional layer of transported particles (a liquid-like or ‘soft’ bed [55]) develops as the bed surface becomes completely mobile (‘stage-3’ bedload transport [13], Movie S4). This liquid-like bed hinders particles moving over it from reaching the disturbed-flow region near the quasi-static-bed surface as they tend to rebound from the liquid-bed sur-

face (Movie S4). Hence, these particles can remain extended periods of time in the nearly-undisturbed-flow region, leading to an increase of \bar{v}_x with Θ . This point is further supported by Fig. 7a, which shows that, for fully impact-sustained conditions, the beginning increase of \bar{v}_x (Fig. 7b) approximately coincides with a beginning increase of the effective location z_r of energetic particle rebounds relative to the quasi-static bed location z_s :

$$\Delta z_r = z_r - z_s, \quad (10)$$

where z_s is defined through

$$\mu(z_s) = 0.7\mu_b. \quad (11)$$

This definition accounts for potential dependencies of z_s on the contact friction coefficient μ^c . For a typical value $\mu_b = 0.6$, it corresponds to $\mu(z_s) = 0.42$, consistent with the definition of the quasi-static bed surface applied in previous studies of bedload transport [67].

VI. DISCUSSIONS AND CONCLUSIONS

Our study challenges the paradigm that sediment transport mediated by water [13, 22, 32] or heavy air [10, 48, 49, 97], like on Venus and Titan, is sustained through direct fluid entrainment of bed particles. Using direct sediment transport simulations in a Newtonian fluid for a wide range of the particle-fluid-density ratio s , Galileo number Ga , and Shields number Θ , we have shown that the effective horizontal near-bed particle velocity (‘bed velocity’) in natural units (V_b/\sqrt{gd})

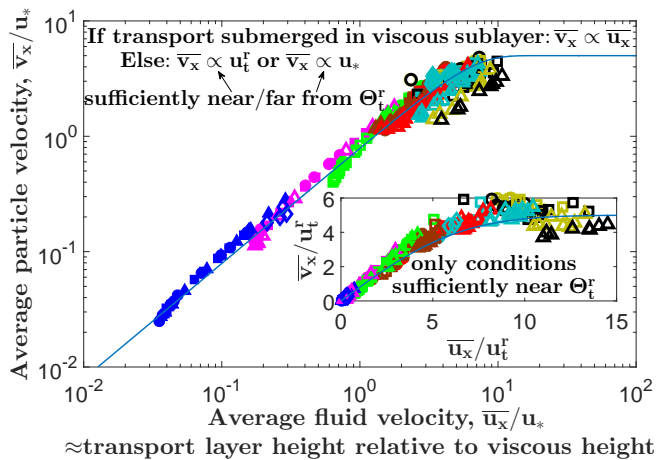


FIG. 6. Average particle velocity \bar{v}_x versus average fluid velocity \bar{u}_x , both rescaled by the fluid shear velocity u_* , for various s , Ga , and Θ . Inset: The same in linear-linear scale, but both velocities rescaled by the fluid shear velocity at the threshold (u_t^r). Among the fully impact-sustained simulation cases, only those corresponding to the linear transport rate regime are shown in the inset (see text). The solid lines correspond to $\bar{v}_x/u_*^{\text{typ}} = 5.0\sqrt{1 - \exp[-0.025(\bar{u}_x/u_*^{\text{typ}})^2]}$, where $u_*^{\text{typ}} = u_*$ (main figure) or $u_*^{\text{typ}} = u_t^r$ (inset). For symbol legend, see Fig. 2.

becomes a universal constant when the ‘impact number’ $\text{Im} = \text{Ga}\sqrt{s+0.5} \gtrsim 20$ or $\Theta \gtrsim 5/\text{Im}$ (Figs. 3b,c). This result indicates that sediment transport is sustained solely through particle-bed impacts when $\text{Im} \gtrsim 20$, which includes nearly all relevant sediment transport regimes. Only sufficiently viscous bedload transport is partially ($\text{Im} \lesssim 20$ and $\Theta \lesssim 5/\text{Im}$) or fully ($\text{Im} \lesssim 20$ and $\Theta \lesssim 1/\text{Im}$) sustained through direct fluid entrainment. However, visualizations of the simulations indicate that the quality of impact entrainment in turbulent bedload is quite different from the one in saltation transport, known as ‘splash’. While in saltation transport, the entrained particles are literally ejected from the bed, in bedload transport they are rather dragged out of their traps by the impacting particles (Fig. 1 and Movies S1-S3). Note that, for fully impact-sustained transport, the impact number scales as $\text{Im} = (s+0.5)d\sqrt{gd}/\nu \propto (s+0.5)dV_b/\nu$ and may therefore be interpreted as a Stokes number associated with particle-bed impacts.

Our study further challenges the very common assumption in saltation transport modeling that the entire particle motion can be represented by particles moving in identical periodic trajectories [7, 9, 38, 46, 48, 49, 73, 98–105]. If this assumption was true, the transport-layer-averaged horizontal particle velocity \bar{v}_x would be bounded between the horizontal velocities at take-off and impact and thus be approximately proportional to the slip velocity $\langle v_x \rangle(z_r)$, which is the average particle velocity at the location of the bed surface (z_r). However, we

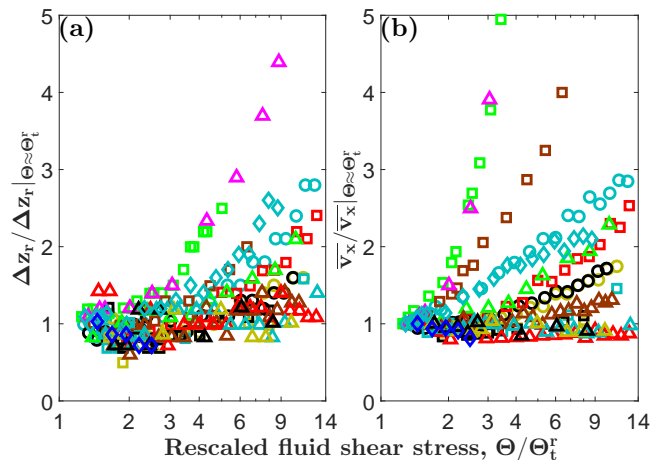


FIG. 7. (a) Rescaled effective location of energetic rebounds relative to the quasi-static bed $\Delta z_r/\Delta z_r|_{\Theta \approx \Theta_t^r}$ versus rescaled dimensionless fluid shear stress Θ/Θ_t^r for fully impact-sustained conditions. (b) Rescaled average particle velocity $\bar{v}_x/\bar{v}_x|_{\Theta \approx \Theta_t^r}$ versus Θ/Θ_t^r for fully impact-sustained conditions. For symbol legend, see Fig. 2.

find that \bar{v}_x scales with the fluid velocity within the transport layer (Fig. 6) and generally not with $\langle v_x \rangle(z_r)$ nor V_b (Fig. 5). We also find that the locally averaged vertical particle velocity $\sqrt{\langle v_z^2 \rangle}(z)$ increases exponentially with elevation z near the bed surface (Fig. 2b), whereas an identical-trajectory model necessarily predicts a decrease. These discrepancies are evidence for a separation of particle velocity scales, which was already pointed out for saltation transport in a previous study (Fig. 21 of Ref. [9]). Near the bed surface, the average particle velocity is dominated by a comparably slow species of particle (‘reptons’ [71] or ‘leapers’/‘creepers’ [55]), whereas at larger elevations that cannot be reached by the slow species, a comparably fast species dominates (‘saltons’ [55, 71]). This being said, identical-trajectory representations of sediment transport do have their uses. For instance, they seem to give valuable insights into the physics of sediment transport cessation [48–50].

Finally, for fully impact-sustained transport, our study predicts a relatively strong negative feedback of the particle motion on the flow when the dimensionless fluid shear stress is sufficiently close to Θ_t^r . As a consequence, \bar{v}_x , which is controlled by the flow, remains approximately constant with Θ , leading to a linear scaling of the sediment transport rate ($Q \propto \Theta - \Theta_t^r$). However, for turbulent bedload transport, this linear scaling becomes non-linear slightly above the threshold ($\Theta \approx 2\Theta_t^r$, see Fig. 4) due to a sudden drop in the relative feedback strength, which is associated with the formation of a liquid-like bed of particles on top of the quasi-static bed surface (Fig. 7).

Our numerical finding that steady turbulent bedload transport is fully sustained through entrainment by particle-bed impacts may be criticized because the simulations neglect a number of items that are deemed to

have a significant influence on bedload transport: they neglect the hindrance effect (i.e., an increase of the average fluid drag force at large particle concentrations), are quasi-two-dimensional, and do only account for the mean turbulent flow, but not for turbulent fluctuations around the mean, which are known to be crucial for the initiation of bedload transport [28–30]. However, we believe that our finding is robust because our simulations quantitatively reproduce measurements of bedload transport cessation thresholds [50], which would not be expected if these neglected items played a crucial role for sustaining steady bedload transport. Our reasoning is supported by Ref. [67], who compared three-dimensional bedload transport simulations with and without turbulent fluctuations. Their Fig. 6 indicates that, although the initiation threshold is strongly affected by turbulent fluctuations, the cessation threshold is nearly unaffected because the extrapolation of the simulated transport rates to vanishing transport remains nearly the same.

Appendix A: Movie captions

1. Movie S1

Time evolution of the simulated particle-fluid system for $s = 2000$, $\text{Ga} = 20$, and $\Theta \simeq 2.1\Theta_t^r$, considering weakly-damped binary collisions ($e = 0.9$). The flow velocity is shown as a background color with warm colors corresponding to high velocities and cold colors to small velocities. The horizontal and vertical axes are measured in mean particle diameters. Only 1/4 of the simulated horizontal domain is shown, which is why there are occasions at which no moving particle can be observed. This is an example for saltation transport, which is predominantly sustained through particle-bed impact entrainment. One can see that impacting particles tend to eject surface particles.

2. Movie S2

Time evolution of the simulated particle-fluid system for $s = 2.65$, $\text{Ga} = 20$, and $\Theta \simeq 1.7\Theta_t^r$, considering binary collisions that are nearly fully damped by the lubrication force ($e = 0.01$). The flow velocity is shown as a background color with warm colors corresponding to high velocities and cold colors to small velocities. The hori-

zontal and vertical axes are measured in mean particle diameters. Only 1/4 of the simulated horizontal domain is shown, which is why there are occasions at which no moving particle can be observed. This is an example for turbulent bedload transport, which is predominantly sustained through particle-bed impact entrainment. One can see that impacting particles tend to drag surface particles out of they traps.

3. Movie S3

Time evolution of the simulated particle-fluid system for $s = 2000$, $\text{Ga} = 20$, and $\Theta \simeq 17.1\Theta_t^r$, considering weakly-damped binary collisions ($e = 0.9$). The flow velocity is shown as a background color with warm colors corresponding to high velocities and cold colors to small velocities. The horizontal and vertical axes are measured in mean particle diameters. Only 1/4 of the simulated horizontal domain is shown, which is why there are occasions at which no moving particle can be observed. This is an example for saltation transport, which is predominantly sustained through particle-bed impact entrainment. One can see that impacting particles tend to eject surface particles.

4. Movie S4

Time evolution of the simulated particle-fluid system for $s = 2.65$, $\text{Ga} = 20$, and $\Theta \simeq 13.8\Theta_t^r$, considering binary collisions that are nearly fully damped by the lubrication force ($e = 0.01$). The flow velocity is shown as a background color with warm colors corresponding to high velocities and cold colors to small velocities. The horizontal and vertical axes are measured in mean particle diameters. Only 1/4 of the simulated horizontal domain is shown. This is an example for turbulent bedload transport, which is predominantly sustained through particle-bed impact entrainment. However, it is impossible to determine single entrainment events because several layers of the bed are in continuous motion. These layers constitute the liquid-like bed, and it can be seen that energetic particles tend to rebound from its top.

ACKNOWLEDGMENTS

We acknowledge support from grant National Natural Science Foundation of China (No. 11550110179).

-
- [1] M. Yalin, *Mechanics of Sediment Transport* (Pergamon Press, Oxford, 1977).
 - [2] W. H. Graf, *Hydraulics of sediment transport* (Water Resources Publications, Littleton, 1984).
 - [3] L. C. van Rijn, *Principles of sediment transport in rivers, estuaries and coastal seas* (Aqua Publications,

Amsterdam, 1993).

- [4] P. Y. Julien, *Erosion and Sedimentation* (Cambridge University Press, Cambridge, 1998).
- [5] M. H. Garcia, *Sedimentation engineering: processes, measurements, modeling, and practice* (American Society of Civil Engineers, 2007).

- [6] M. C. Bourke, N. Lancaster, L. K. Fenton, E. J. R. Parteli, J. R. Zimelman, and J. Radebaugh, “Extraterrestrial dunes: An introduction to the special issue on planetary dune systems,” *Geomorphology* **121**, 1–14 (2010).
- [7] R. A. Bagnold, *The physics of blown sand and desert dunes* (Methuen, New York, 1941).
- [8] Y. Shao, *Physics and modelling of wind erosion* (Kluwer Academy, Dordrecht, Amsterdam, 2008).
- [9] O. Durán, P. Claudin, and B. Andreotti, “On aeolian transport: Grain-scale interactions, dynamical mechanisms and scaling laws,” *Aeolian Research* **3**, 243–270 (2011).
- [10] J. F. Kok, E. J. R. Parteli, T. I. Michaels, and D. Bou Karam, “The physics of wind-blown sand and dust,” *Reports on Progress in Physics* **75**, 106901 (2012).
- [11] A. Valance, K. R. Rasmussen, A. Ould El Moctar, and P. Dupont, “The physics of aeolian sand transport,” *Comptes Rendus Physique* **16**, 105–117 (2015).
- [12] P. Frey and M. Church, “How river beds move,” *Science* **325**, 1509–1510 (2009).
- [13] P. Frey and M. Church, “Bedload: a granular phenomenon,” *Earth Surface Processes and Landforms* **36**, 58–69 (2011).
- [14] A. F. Shields, *Application of Similarity Principles and Turbulence Research to Bedload Movement (English translation of the original German manuscript)*, 167 (Hydrodynamics Laboratory, California Institute of Technology, Pasadena, Calif, 1936).
- [15] B. D. Ward, “Relative density effects on incipient bed movement,” *Water Resources Research* **5**, 1090–1096 (1969).
- [16] L. C. van Rijn, “Sediment transport, part i: Bed load transport,” *Journal of Hydraulic Engineering* **110**, 1431–1456 (1984).
- [17] J. M. Buffington and D. R. Montgomery, “A systematic analysis of eight decades of incipient motion studies, with special reference to gravel-bedded rivers,” *Water Resources Research* **33**, 1993–2029 (1997).
- [18] P. R. Wilcock, “Two-fraction model of initial sediment motion in gravel-bed rivers,” *Science* **280**, 410–412 (1998).
- [19] J. M. Buffington, “The legend of a. f. shields,” *Journal of Hydraulic Engineering* **125**, 376–387 (1999).
- [20] S. Dey, “Sediment threshold,” *Applied Mathematical Modelling* **23**, 399–417 (1999).
- [21] S. Dey, “Threshold of sediment motion on combined transverse and longitudinal sloping beds,” *Journal of Hydraulic Research* **41**, 405–415 (2003).
- [22] D. Paphitis, “Sediment movement under unidirectional flows: an assessment of empirical threshold curves,” *Coastal Engineering* **43**, 227–245 (2001).
- [23] Z. Cao, G. Pender, and J. Meng, “Explicit formulation of the shields diagram for incipient motion of sediment,” *Journal of Hydraulic Engineering* **132**, 1097–1099 (2006).
- [24] S. Vollmer and M. G. Kleinhans, “Predicting incipient motion, including the effect of turbulent pressure fluctuations in the bed,” *Water Resources Research* **43**, W05410 (2007).
- [25] A. A. Beheshti and B. Ataie-Ashtiani, “Analysis of threshold and incipient conditions for sediment movement,” *Coastal Engineering* **55**, 423–430 (2008).
- [26] S. Dey and A. Papanicolaou, “Sediment threshold under stream flow: A state-of-the-art review,” *Water Engineering* **12**, 45–60 (2008).
- [27] A. Recking, “Theoretical development on the effects of changing flow hydraulics on incipient bed load motion,” *Water Resources Research* **45**, W04401 (2009).
- [28] P. Diplas, C. L. Dancey, A. O. Celik, M. Valyrakis, K. Greer, and T. Akar, “The role of impulse on the initiation of particle movement under turbulent flow conditions,” *Science* **322**, 717–720 (2008).
- [29] M. Valyrakis, P. Diplas, C. L. Dancey, K. Greer, and A. O. Celik, “Role of instantaneous force magnitude and duration on particle entrainment,” *Journal of Geophysical Research* **115**, F02006 (2010).
- [30] M. Valyrakis, P. Diplas, and C. L. Dancey, “Entrainment of coarse particles in turbulent flows: An energy approach,” *Journal of Geophysical Research* **118**, 42–53 (2013).
- [31] H. Lee, M. Y. Ha, and S. Balachandar, “Work-based criterion for particle motion and implication for turbulent bed-load transport,” *Physics of Fluids* **24**, 116604 (2012).
- [32] M. Houssais, C. P. Ortiz, D. J. Durian, and D. J. Jerolmack, “Onset of sediment transport is a continuous transition driven by fluid shear and granular creep,” *Nature Communications* **6**, 6527 (2015).
- [33] S. Z. Ali and S. Dey, “Hydrodynamics of sediment threshold,” *Physics of Fluids* **28**, 075103 (2016).
- [34] G. Maniatis, T. B. Hoey, M. A. Hassan, J. Sventek, R. Hodge, T. Drysdale, M. Valyrakis, and M. ASCE, “Calculating the explicit probability of entrainment based on inertial acceleration measurements,” *Journal of Hydraulic Engineering*, 04016097 (2016).
- [35] L. Roušar, Z. Zchoval, and P. Julien, “Incipient motion of coarse uniform gravel,” *Journal of Hydraulic Research* **54**, 615–630 (2016).
- [36] R. A. Bagnold, “The transport of sand by wind,” *The Geographical Journal* **89**, 409–438 (1937).
- [37] R. A. Bagnold, “The nature of saltation and “bed-load” transport in water,” *Proceedings of the Royal Society London Series A* **332**, 473–504 (1973).
- [38] J. E. Ungar and P. K. Haff, “Steady state saltation in air,” *Sedimentology* **34**, 289–299 (1987).
- [39] R. S. Anderson and P. K. Haff, “Simulation of eolian saltation,” *Science* **241**, 820–823 (1988).
- [40] R. S. Anderson and P. K. Haff, “Wind modification and bed response during saltation of sand in air,” *Acta Mechanica Supplementum* **1**, 21–51 (1991).
- [41] I. K. McEwan and B. B. Willetts, “Numerical model of the saltation cloud,” *Acta Mechanica Supplementum* **1**, 53–66 (1991).
- [42] I. K. McEwan and B. B. Willetts, “Adaptation of the near-surface wind to the development of sand transport,” *Journal of Fluid Mechanics* **252**, 99–115 (1993).
- [43] J. F. Kok, “Difference in the wind speeds required for initiation versus continuation of sand transport on mars: Implications for dunes and dust storms,” *Physical Review Letters* **104**, 074502 (2010).
- [44] J. F. Kok, “An improved parameterization of wind blown sand flux on mars that includes the effect of hysteresis,” *Geophysical Research Letters* **37**, L12202 (2010).
- [45] T. Pächt, J. F. Kok, and H. J. Herrmann, “The apparent roughness of a sand surface blown by wind from an

- analytical model of saltation,” *New Journal of Physics* **14**, 043035 (2012).
- [46] J. T. Jenkins and A. Valance, “Periodic trajectories in aeolian sand transport,” *Journal of Fluid Mechanics* **26**, 073301 (2014).
- [47] M. V. Carneiro, K. R. Rasmussen, and H. J. Herrmann, “Bursts in discontinuous aeolian saltation,” *Scientific Reports* **5**, 1–8 (2015).
- [48] D. Berzi, J. T. Jenkins, and A. Valance, “Periodic saltation over hydrodynamically rough beds: aeolian to aquatic,” *Journal of Fluid Mechanics* **786**, 190–209 (2016).
- [49] D. Berzi, A. Valance, and J. T. Jenkins, “The threshold for continuing saltation on earth and other solar system bodies,” *Journal of Geophysical Research: Earth Surface* (2017).
- [50] T. Pähz, and O. Durán, “Unified threshold model suggests sediment transport by wind on triton, pluto, and comet 67p,” (2017), <https://arxiv.org/abs/1602.07079>.
- [51] A. H. Clark, M. D. Shattuck, N. T. Ouellette, and C. S. O’Hern, “Onset and cessation of motion in hydrodynamically sheared granular beds,” *Physical Review E* **92**, 042202 (2015).
- [52] A. H. Clark, M. D. Shattuck, N. T. Ouellette, and C. S. O’Hern, “Role of grain dynamics in determining the onset of sediment transport,” *Physical Review Fluids* **2**, 034305 (2017).
- [53] O. Durán, B. Andreotti, and P. Claudin, “Numerical simulation of turbulent sediment transport, from bed load to saltation,” *Physics of Fluids* **24**, 103306 (2012).
- [54] M. V. Carneiro, T. Pähz, and H. J. Herrmann, “Jump at the onset of saltation,” *Physical Review Letters* **107**, 098001 (2011).
- [55] M. V. Carneiro, N. A. M. Araújo, T. Pähz, and H. J. Herrmann, “Midair collisions enhance saltation,” *Physical Review Letters* **111**, 058001 (2013).
- [56] C. Ji, A. Munjiza, E. Avital, J. Ma, and J. J. R. Williams, “Direct numerical simulation of sediment entrainment in turbulent channel flow,” *Physics of Fluids* **25**, 056601 (2013).
- [57] O. Durán, B. Andreotti, and P. Claudin, “Turbulent and viscous sediment transport a numerical study,” *Advances in Geosciences* **37**, 73–80 (2014).
- [58] O. Durán, P. Claudin, and B. Andreotti, “Direct numerical simulations of aeolian sand ripples,” *Proceedings of the National Academy of Science* **111**, 15665–15668 (2014).
- [59] A. G. Kidanemariam and M. Uhlmann, “Direct numerical simulation of pattern formation in subaqueous sediment,” *Journal of Fluid Mechanics* **750**, R2 (2014).
- [60] A. G. Kidanemariam and M. Uhlmann, “Interface-resolved direct numerical simulation of the erosion of a sediment bed sheared by laminar channel flow,” *International Journal of Multiphase Flow* **67**, 174–188 (2014).
- [61] A. G. Kidanemariam and M. Uhlmann, “Formation of sediment patterns in channel flow: minimal unstable systems and their temporal evolution,” *Journal of Fluid Mechanics* **818**, 716–743 (2017).
- [62] M. W. Schmeekle, “Numerical simulation of turbulence and sediment transport of medium sand,” *Journal of Geophysical Research: Earth Surface* **119**, 1240–1262 (2014).
- [63] B. Vowinkel, T. Kempe, and J. Fröhlich, “Fluid-particle interaction in turbulent open channel flow with fully-resolved mobile beds,” *Advances in Water Resources* **72**, 32–44 (2014).
- [64] S. K. Arolla and O. Desjardins, “Transport modeling of sedimenting particles in a turbulent pipe flow using euler-lagrange large eddy simulation,” *International Journal of Multiphase Flow* **75**, 1–11 (2015).
- [65] T. Pähz, O. Durán, T.-D. Ho, A. Valance, and J. F. Kok, “The fluctuation energy balance in non-suspended fluid-mediated particle transport,” *Physics of Fluids* **27**, 013303 (2015).
- [66] J. J. Derksen, “Simulations of granular bed erosion due to a mildly turbulent shear flow,” *Journal of Hydraulic Research* **53**, 622–632 (2015).
- [67] R. Maurin, J. Chauchat, B. Chareyre, and P. Frey, “A minimal coupled fluid-discrete element model for bed-load transport,” *Physics of Fluids* **27**, 113302 (2015).
- [68] R. Maurin, J. Chauchat, and P. Frey, “Dense granular flow rheology in turbulent bedload transport,” *Journal of Fluid Mechanics* **804**, 490–512 (2016).
- [69] J. R. Finn and M. Li, “Regimes of sediment-turbulence interaction and guidelines for simulating the multiphase bottom boundary layer,” *International Journal of Multiphase Flow* **85**, 278–283 (2016).
- [70] J. R. Finn, M. Li, and S. V. Apte, “Particle based modelling and simulation of natural sand dynamics in the wave bottom boundary layer,” *Journal of Fluid Mechanics* **796**, 340–385 (2016).
- [71] B. Andreotti, “A two-species model of aeolian sand transport,” *Journal of Fluid Mechanics* **510**, 47–70 (2004).
- [72] L. Oger, M. Ammi, A. Valance, and D. Beladjine, “Discrete element method studies of the collision of one rapid sphere on 2d and 3d packings,” *European Physical Journal E* **17**, 467–476 (2005).
- [73] P. Claudin and B. Andreotti, “A scaling law for aeolian dunes on mars, venus, earth, and for subaqueous ripples,” *Earth and Planetary Science Letters* **252**, 30–44 (2006).
- [74] D. Beladjine, M. Ammi, L. Oger, and A. Valance, “Collision process between an incident bead and a three-dimensional granular packing,” *Physical Review E* **75**, 061305 (2007).
- [75] L. Oger, M. Ammi, A. Valance, and D. Beladjine, “Study of the collision of one rapid sphere on 3d packings: Experimental and numerical results,” *Computers and Mathematics with Applications* **55**, 132–148 (2008).
- [76] M. Lämmel, D. Rings, and K. Kroy, “A two-species continuum model for aeolian sand transport,” *New Journal of Physics* **14**, 093037 (2012).
- [77] J. A. Simeonov and J. Calantoni, “Dense granular flow rheology in turbulent bedload transport,” *International Journal of Multiphase Flow* **46**, 38–53 (2012).
- [78] P. Gondret, M. Lance, and L. Petit, “Bouncing motion of spherical particles in fluids,” *Physics of Fluids* **14**, 2803–2805 (2002).
- [79] F. L. Yang and M. L. Hunt, “Dynamics of particle-particle collisions in a viscous liquid,” *Physics of Fluids* **18**, 121506 (2006).
- [80] T. D. Ho, *Etude expérimentale du transport de particules dans une couche limite turbulente*, Ph.D. thesis, University of Rennes, Rennes, France (2012).
- [81] X. Y. Zou, Z. L. Wang, Q. Z. Hao, C. L. Zhang, Y. Z. Liu, and G. R. Dong, “The distribution of velocity and energy of saltating sand grains in a wind tunnel,” *Geo-*

- morphology **36**, 155–165 (2001).
- [82] Z. Dong, Xiaoping Liu, X. Wang, F. Li, and A. Zhao, “Experimental investigation of the velocity of a sand cloud blowing over a sandy surface,” *Earth Surface Processes and Landforms* **29**, 343–358 (2004).
- [83] P. Yang, Z. Dong, G. Qian, W. Luo, and H. Wang, “Height profile of the mean velocity of an aeolian saltating cloud: Wind tunnel measurements by particle image velocimetry,” *Geomorphology* **89**, 320–334 (2007).
- [84] L. Kang, L. Guo, Z. Gu, and D. Liu, “Wind tunnel experimental investigation of sand velocity in aeolian sand transport,” *Geomorphology* **97**, 438–450 (2008).
- [85] K. R. Rasmussen and M. Sørensen, “Vertical variation of particle speed and flux density in aeolian saltation: Measurement and modeling,” *Journal of Geophysical Research* **113**, F02S12 (2008).
- [86] M. Creyssels, P. Dupont, A. Ould El Moctar, A. Valance, I. Cantat, J. T. Jenkins, J. M. Pasini, and K. R. Rasmussen, “Saltating particles in a turbulent boundary layer: experiment and theory,” *Journal of Fluid Mechanics* **625**, 47–74 (2009).
- [87] T. D. Ho, A. Valance, P. Dupont, and A. Ould El Moctar, “Scaling laws in aeolian sand transport,” *Physical Review Letters* **106**, 094501 (2011).
- [88] M. Ouriemi, P. Aussillous, M. Medale, Y. Peysson, and E. Guazzelli, “Determination of the critical shields number for particle erosion in laminar flow,” *Physics of Fluids* **19**, 061706 (2007).
- [89] G. M. Smart, “Sediment transport formula for steep channels,” *Journal of Hydraulic Engineering* **110**, 267–276 (1984).
- [90] E. Lajeunesse, L. Malverti, and F. Charru, “Bed load transport in turbulent flow at the grain scale: Experiments and modeling,” *Journal of Geophysical Research* **115**, F04001 (2010).
- [91] H. Capart and L. Fraccarollo, “Transport layer structure in intense bedload,” *Geophysical Research Letters* **38**, L20402 (2011).
- [92] R. A. Bagnold, “The movement of desert sand,” *Proceedings of the Royal Society London Series A* **157**, 594–620 (1936).
- [93] R. A. Bagnold, “The measurement of sand storms,” *Proceedings of the Royal Society London Series A* **167**, 282–291 (1938).
- [94] K. R. Rasmussen, J. D. Iversen, and P. Rautahemio, “Saltation and wind-flow interaction in a variable slope wind tunnel,” *Geomorphology* **17**, 19–28 (1996).
- [95] R. L. Martin and J. F. Kok, “Wind-invariant saltation heights imply linear scaling of aeolian saltation flux with shear stress,” (2017), <https://arxiv.org/abs/1609.09458>.
- [96] J. R. Mayaud, R. M. Bailey, G. F. S. Wiggs, and C. M. Weaver, “Modelling aeolian sand transport using a dynamic mass balancing approach,” *Geomorphology* **280**, 108–121 (2017).
- [97] D. M. Burr, N. T. Bridges, J. R. Marshall, J. K. Smith, B. R. White, and J. P. Emery, “Higher-than-predicted saltation threshold wind speeds on titan,” *Nature* **517**, 60–63 (2015).
- [98] R. Kawamura, “Study of sand movement by wind,” in *Translated (1965) as University of California Hydraulics Engineering Laboratory Report HEL 2 Berkeley* (1951).
- [99] P. R. Owen, “Saltation of uniform grains in air,” *Journal of Fluid Mechanics* **20**, 225–242 (1964).
- [100] R. J. Kind, “A critical examination of the requirements for model simulation of wind-induced erosion/deposition phenomena such as snow drifting,” *Atmospheric Environment* **10**, 219–227 (1976).
- [101] K. Lettau and H. H. Lettau, “Exploring the world’s driest climate,” in *IES Report*, Vol. 101 (1978) pp. 110–147.
- [102] M. Sørensen, “An analytic model of wind-blown sand transport,” *Acta Mechanica Supplementum* **1**, 67–81 (1991).
- [103] M. Sørensen, “On the rate of aeolian sand transport,” *Geomorphology* **59**, 53–62 (2004).
- [104] G. Sauermann, K. Kroy, and H. J. Herrmann, “A continuum saltation model for sand dunes,” *Physical Review E* **64**, 31305 (2001).
- [105] O. Durán and H. J. Herrmann, “Modelling of saturated sand flux,” *Journal of Statistical Mechanics* **2006**, P07011 (2006).